Supplementary Information

Large Differences in Terrestrial Vegetation Production Derived from Satellite-Based Light Use Efficiency Models. *Remote Sensing*, 2014, 6, 8945–8965

Wenwen Cai [1], Wenping Yuan [1,*], Shunlin Liang [2,3], Shuguang Liu [4], Wenjie Dong [1], Yang Chen [1], Dan Liu [1] and Haicheng Zhang [1]

[1] State Key Laboratory of Earth Surface Processes and Resource Ecology,
  Beijing Normal University, Beijing 100875, China;
  E-Mails: caiwenwen@mail.bnu.edu.cn (W.C.); dongwj@bnu.edu.cn (W.D.);
  cheny0323@163.com (Y.C.); liu.dan@mail.bnu.edu.cn (D.L.); sysuzhaicheng@163.com (H.Z.)
[2] State Key Laboratory of Remote Sensing Science, College of Global Change and Earth System
  Science, Beijing Normal University, Beijing 100875, China; E-Mail: sliang@umd.edu
[3] Department of Geographical Sciences, University of Maryland, College Park, MD 20742, USA
[4] Geospatial Science Center of Excellence, South Dakota State University, 1021 Medary Ave, Wecota
  Hall 115, Box 506B, Brookings, SD 57007, USA; E-Mail: shuguang.liu@yahoo.com

* Author to whom correspondence should be addressed; E-Mail: yuanwpcn@126.com;
  Tel.: +86-10-58-807-715; Fax: +86-10-58-803-002.

1. Abbreviations

Table S1. The abbreviations used in this supplementary online material [S1–S9].

Abbreviation	Full name
LUE	Light Use Efficiency
GPP	Gross Primary Productivity
PAR	Photosynthetically Active Radiation
Rn	Net radiation
Ta	Average air temperature
T_{min}	Minimum air temperature
ET	Evapotranspiration
PET	Potential Evapotranspiration

Table S1. *Cont.*

Abbreviation	Full name
VPD	Vapor Pressure Deficit
LSWI	Land Surface Water Index
NDVI	Normalized Difference Vegetation Index
EVI	Enhanced Vegetation Index
FPAR	the Fraction of absorbed Photosynthetically Active Radiation
CASA	Carnegie–Ames–Stanford Approach [S1]
CFix	Carbon Fixation model [S2]
CFlux	Carbon Flux model [S3,S4]
EC-LUE	Eddy Covariance-Light Use Efficiency model [S5,S6]
MODIS	Moderate Resolution Imaging Spectroradiometer GPP algorithm [S7]
VPM	Vegetation Photosynthesis Model [S8]
VPRM	Vegetation Photosynthesis and Respiration Model [S9]

2. LUE Models

2.1. Model Description and Equations

We used seven LUE models in the present study, including CASA, CFix, CFlux, EC-LUE, MODIS, VPM and VPRM models. The relative abbreviations were shown in the above Table S1. These models (Table S2) were briefly described below.

Table S2. Summary of the seven LUE models and input variables at global scale.

LUE Models	Meteorology Data and Vegetation Indices Used in Each Models
CASA	PAR, Ta, ET, PET, NDVI
CFix	PAR, Ta, ET, PET, NDVI
CFlux	PAR, T_{min}, VPD, ET, PET, Cloudiness, FPAR
EC-LUE	PAR, T_{min}, ET, Rn, NDVI
MODIS	PAR, Ta, VPD, FPAR
VPRM	PAR, Ta, LSWI, EVI
VPRM	PAR, Ta, LSWI, EVI

3. CASA Model

CASA model runs on a monthly step to directly simulate vegetation net primary production, and GPP was obtained through an average ratio 0.5 of net primary production to GPP in this study [S10]. CASA converts the absorbed radiation to organic carbon through a globally universal potential LUE (LUE_{max}) which is constrained by spatial- and temporally varied temperature and water. The complete expression of GPP estimation by CASA therefore is:

$$GPP = PAR \times FPAR \times LUE_{max} \times T_{s1} \times T_{s2} \times W_s \times 2 \tag{S1}$$

where T_{s1} and T_{s2} are two scalars for the effects of temperature on potential LUE, respectively. W_s is the scalar for the effect of moisture on LUE_{max}. CASA utilizes remotely-sensed NDVI to quantify FPAR according to the linear relationship between FPAR and Simple Ratio (SR) vegetation index:

$$SR = (1 + NDVI)/(1 - NDVI) \tag{S2}$$

$$FPAR = min\left(SR/(SR - SR_{min}) - SR_{min}/(SR_{max} - SR_{min}), 0.95\right) \tag{S3}$$

The temperature scalars T_{s1} and T_{s2} consider the limitation of extreme and sub-optimal temperature on vegetation photosynthesis, respectively. Potential LUE declines under very high or very low temperatures and also decreases when temperature is above or below the optimum temperature T_{opt}. T_{opt} is defined as the air temperature in the month when NDVI reaches its maximum value for the whole year. The moisture scalar W_s quantifies the limitation of soil water on vegetation photosynthesis. ET and PET are a practical choice used to calculate W_s. The three environmental stress scalars are formulated as:

$$T_{s1} = 0.8 + 0.02 \times T_{opt} - 0.0005 \times T_{opt} \times T_{opt} \tag{S4}$$

$$T_{s2} = 1.1919 \left/ \left(\left(1 + e^{0.2 \times (T_{opt} - 10 - T_a)}\right) \middle/ \left(1 + e^{0.3 \times (-T_{opt} - 10 + T_a)}\right) \right) \right. \tag{S5}$$

$$W_s = 0.5 + 0.5 \times (ET/PET) \tag{S6}$$

4. CFix Model

CFix model is a daily Monteith type parametric model driven by air temperature, radiation, moisture and FPAR:

$$GPP = PAR \times FPAR \times LUE_w \times \rho(T_a) \times CO_2 fert \tag{S7}$$

where LUE_w is the light use efficiency considering the effect of water on photosynthesis. The scalars $\rho(T_a)$ and $CO_2 fert$ models the dependency of GPP on air temperature and atmospheric CO_2 fertilization, respectively. Both are normalized to the range 0 and 1. The FPAR is quantified by a linear relationship which is insensitive to the pixel heterogeneity [S11]:

$$FPAR = 0.8642 \times NDVI - 0.0814 \tag{S8}$$

The temperature scalar $\rho(T_a)$ simulates the thermodynamic properties of the carboxylation/oxygenation reactions of Rubisco (photosynthesis) [S12]. The $CO_2 fert$ quantifies the increase in the proportion of carbon uptake by vegetation when CO_2 concentration rises above its atmospheric background level.

$$\rho(T_a) = e^{C_l - \Delta H_{a,P}/(R_g \times T_a)} \left/ \left(1 + e^{(\Delta S \times T - \Delta H_{d,P})/(R_g \times T_a)} \right) \right. \tag{S9}$$

$$CO_2 fert = \frac{[CO_2] - \dfrac{[O_2]}{2s}}{[CO_2]^{ref} - \dfrac{[O_2]}{2s}} \frac{K_m \times (1 + \dfrac{[O_2]}{K_0}) + [CO_2]^{ref}}{K_m \times (1 + \dfrac{[O_2]}{K_0}) + [CO_2]} \tag{S10}$$

where C_l, ΔS, $\Delta H_{a,P}$, $\Delta H_{d,P}$, R_g at the temperature response equation $\rho(T_a)$ are 21.77, 704.98 J·K^{-1}·mol^{-1}, 52,750 J·mol^{-1}, 211,000 J·mol^{-1}, 8.31 J·K^{-1}·mol^{-1} according to Veroustraete *et al.* [S2]; the parameter values of s, K_m, K_o, [CO2]^{ref} are 2550, 948, 30 and 281 ppm respectively. In this study, [O$_2$] was set to 209,000 ppm, and [CO$_2$] was set to be annual mean global carbon dioxide concentration using

measurements of weekly air samples from the Cooperative Global Air Sampling network (http://www.esrl.noaa.gov/gmd/ccgg/trends/global.html).

The LUE_w considers the effect of water availability especially water limitation on the process of photosynthesis [S13]. In the original CFix model, the water limited light use efficiency LUE_w is formulated based on soil and atmospheric moisture, since both affect water availability for photosynthesis. Considering the difficulty and large uncertainty in simulating soil moisture at large scale, we only adapted the impacts of atmospheric moisture on LUE_{max} in this study, and simplified the GPP dependency on water limitation as following:

$$LUE_w = LUE_{min} + F_a \times \left(LUE_{max} - LUE_{min} \right) \tag{S11}$$

where LUE_{min} and LUE_{max} are the minimum and maximum LUE, respectively. F_a is a coefficient adjusting the strength of water limitation.

5. CFlux Model

The input variables of CFlux model include daily meteorological data and satellite-derived information on land cover, stand age and FPAR [S3,S4]. The process of GPP estimation at a daily time step is realized by integrating the effects of daily minimum temperature, daytime average VPD, cloudiness, soil water status, and stand age on potential LUE, which are expressed as:

$$GPP = PAR \times FPAR \times LUE_r \tag{S12}$$

$$LUE_r = LUE_{base} \times S_{Tmin} \times min\left\{ S_{vpd}, S_{sw} \right\} \times S_{age} \tag{S13}$$

$$LUE_{base} = \left(LUE_{max} - LUE_{cs} \right) \times S_{CI} + LUE_{cs} \tag{S14}$$

where LUE_r is the realized light use efficiency, LUE_{cs} is the light use efficiency under clear sky condition. S_{CI} is the cloudiness scalar and cloudiness is determined by the ratio of incident PAR to potential PAR [S3]. The minimum temperature scalar S_{Tmin} and daytime average VPD scalar S_{vpd} are adopted from the MODIS GPP algorithm. The scalar for the influence of soil water S_{sw} is based on the ratio of current soil water content to soil water holding capacity. When the ratio is above 0.5, S_{sw} is set to 1. When the ratio is below 0.5 there is a linear ramp from S_{sw} of 1 to S_{sw} of 0 as the ratio hits 0. We simplified the simulations of soil moisture and used evaporative fraction (EF) to indicate S_{SW}. S_{age} is the stand age scalar, which is a unique feature of CFlux model for forests, due to the reduced productivity observed in older stands. However, it is difficult to derive stand age information over large scale. The S_{age} scalar is therefore simplified to 1 when estimating GPP at global scale in our study.

6. EC-LUE Model

EC-LUE model is a light-use-efficiency daily GPP model based on eddy covariance measurements [S5]. It is driven by only four variables: NDVI, PAR, air temperature, and the Bowen ratio of sensible to latent heat flux. At large scale, Bowen ratio is substituted by the ratio of latent heat to net radiation [S6].

$$GPP = PAR \times FPAR \times LUE_{max} \times min\left(T_s, W_s \right) \tag{S15}$$

$$FPAR = 1.24 \times NDVI - 0.618 \tag{S16}$$

$$T_s = \frac{\left(T_a - T_{min}\right) \times \left(T_a - T_{max}\right)}{\left(T_a - T_{min}\right) \times \left(T_a - T_{max}\right) - \left(T_a - T_{opt}\right)^2}$$ (S17)

$$W_s = LE/R_n$$ (S18)

where T_s is the temperature scalar, quantified by daily air temperature combined with the minimum (T_{min}), maximum (T_{max}) and optimum (T_{opt}) air temperatures for photosynthesis. The calibrated values for T_{min}, T_{max}, and T_{opt} are 0, 40, 20.33 °C, respectively [S5]. If air temperature falls below T_{min} or rises beyond T_{max}, T_s is set to 0. R_n is net radiation and the latent heat flux LE is estimated by the revised Remote Sensing–Penman Monteith model (the revised RS-PM) [S6]. The minimum value of T_s and W_s is employed to decline potential LUE, given the assumption that light use efficiency is only affected by the most limiting factor at any given time at location (Liebig's Law).

7. MODIS GPP Algorithm

MODIS GPP algorithm integrates MODIS remote sensing products and DAO (NASA Data Assimilation Office) meteorological data to estimate global GPP based on Monteith's LUE theory [S7]:

$$GPP = PAR \times FPAR \times LUE_{max} \times T_s \times W_s$$ (S19)

$$T_s = \begin{cases} 0 & TMIN < TMIN_{min} \\ \dfrac{TMIN - TMIN_{min}}{TMIN_{max} - TMIN_{min}} & TMIN_{min} < TMIN < TMIN_{max} \\ 1 & TMIN > TMIN_{max} \end{cases}$$ (S20)

$$W_s = \begin{cases} 0 & VPD > VPD_{max} \\ \dfrac{VPD_{max} - VPD}{VPD_{max} - VPD_{min}} & VPD_{min} < VPD < VPD_{max} \\ 1 & VPD < VPD_{min} \end{cases}$$ (S21)

where FPAR is the fraction of PAR absorbed by vegetation canopy, provided by MODIS land product MOD15A2. T_s is the attenuation scalar of daily minimum air temperature and it considers the reduction in the potential LUE due to stomata closure at cold night temperature. W_s is the attenuation scalar of the daytime average VPD which declines LUE_{max} through close stomata at very high VPD. LUE_{max} is used biome dependent values, which implies different photosynthetic ability among plant functional types.

8. VPM Model

VPM model is a satellite-based light use efficiency approach to estimate GPP based on conceptual partition of non-photosynthetically active vegetation and photosynthetically active vegetation within a canopy [S8]. The VPM model is realized as:

$$GPP = PAR \times FPAR \times LUE_{max} \times T_s \times W_s \times P_s$$ (S22)

where FPAR is the fractional of PAR absorbed by photosynthetically active vegetation, which is quantified by the linear relationship with EVI with slope of 1 and intercept of 0. LUE_{max} is affected by

temperature, water, and leaf phenology. The temperature scalar T_s is estimated at each time step, using the equation developed for the Terrestrial Ecosystem Model (Equation (18)) [S14]. The effect of water on plant photosynthesis W_s uses a satellite-derived water index LSWI to estimate the seasonal dynamics of water availability:

$$W_s = \frac{1 + LSWI}{1 + LSWI_{max}} \tag{S23}$$

$$LSWI_{max} = \frac{\rho_{NIR} - \rho_{SWIR}}{\rho_{NIR} + \rho_{SWIR}} \tag{S24}$$

where ρ_{NIR} and ρ_{SWIR} is the surface reflectance at the near-infrared and shortwave band, respectively. MODIS surface reflectance product (MOD09A1) can be used to derive LSWI. $LSWI_{max}$ is the maximum LSWI within the plant growing season. When multi-year LSWI data are available, the mean LSWI values over multiple years at individual temporal points (daily, weekly or 10-day) are calculated, and then the maximum LSWI value within the photosynthetically active period is selected as $LSWI_{max}$.

In the VPM model, P_s is used to account for the effect of leaf age on photosynthesis at canopy level, but it is set to be dependent only on life expectancy of leaves. The calculation of P_s is therefor only for a canopy that is dominated by leaves with a life expectancy of 1 year (one growing season). During the period of bud burst to leaf full expansion and during the time of leaf full expansion to senescence, P_s is formulated as:

$$P_s = \frac{1 + LSWI}{2} \tag{S25}$$

The dates for the three phases of phenology (bud burst, full canopy, and senescence) were obtained using an EVI seasonal threshold similar to that of the MODIS phenology product (MOD12Q2) [S15]. Thus for large-scale application of VPM model, MODIS phenology can be used directly.

9. VPRM Model

VPRM model is a satellite-based carbon assimilation LUE model to estimate GPP using meteorological data and satellite-derived EVI and LSWI data [S9]. The VPRM is developed from VPM model by adding a nonlinear radiation dependency of the potential LUE:

$$GPP = PAR \times FPAR \times \frac{1}{\left(1 + PAR/PAR_0\right)} \times LUE_{max} \times T_s \times W_s \times P_s \tag{S26}$$

where PAR_0 is the half-saturation value.

10. Model Parameterization

Fifty percent of the 157 FLUXNET sites were randomly selected to calibrate model parameters and the remaining sites were used to validate models. This parameterization process was repeated until all possible combinations of the 50% sites were achieved. We then simulated global terrestrial GPP using the seven LUE models each with the mean values of the calibrated parameters and global input variables described in Section 2.2 in the main text. The sites information was listed in Yuan *et al.* [S16].

Figure S1. Distribution of climatic constraints to GPP estimated by CASA model (**a**) Spatial patterns of correlation of annual PAR (**b**); annual mean temperature (**c**); and annual ET (**d**) with annual GPP; (a) is transformed from (b) to (d). The later three data are linearly stretched between 0 and 255, and assigned to Green (radiation (b)), Blue (temperature (c)) and Red (water (d)) for RGB display in (a). The interactions of the three primary color produce: Cyan (temperature and radiation), Magenta (water and temperature) and Yellow (water and radiation).
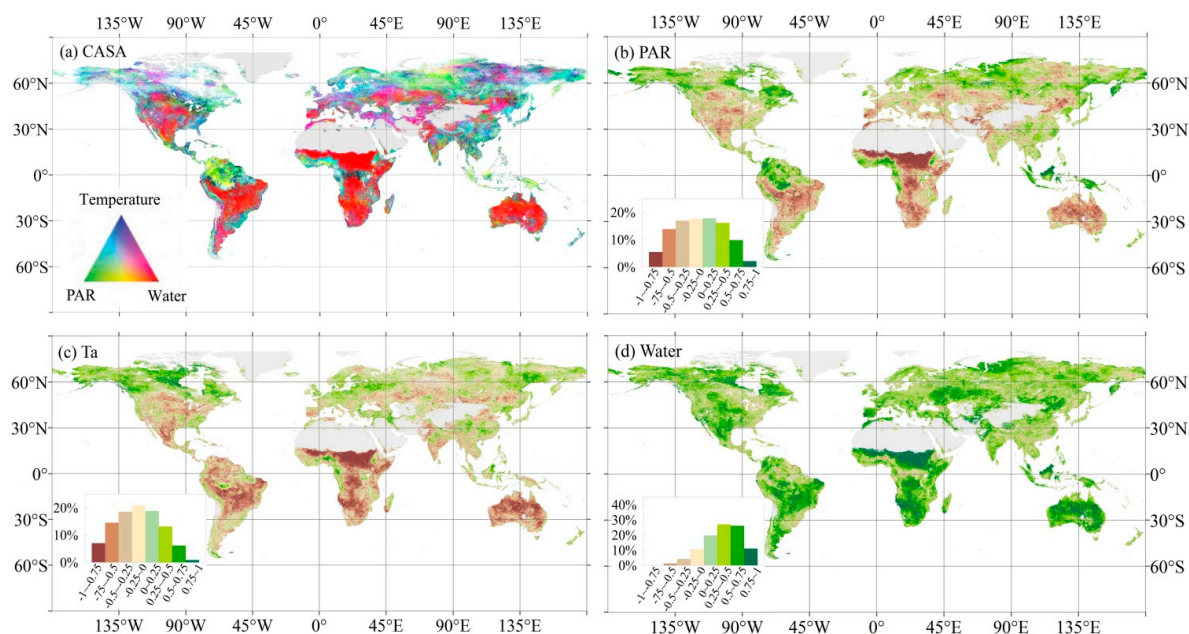
Figure S2. Distribution of climatic constraints to GPP estimated by CFix model (**a**). Spatial patterns of correlation of annual PAR (**b**); annual mean temperature (**c**); and annual ET (**d**) with annual GPP; (a) is transformed from (b) to (d). The later three data are linearly stretched between 0 and 255, and assigned to Green (radiation (b)), Blue (temperature (c)) and Red (water (d)) for RGB display in (a). The interactions of the three primary color produce: Cyan (temperature and radiation), Magenta (water and temperature) and Yellow (water and radiation).
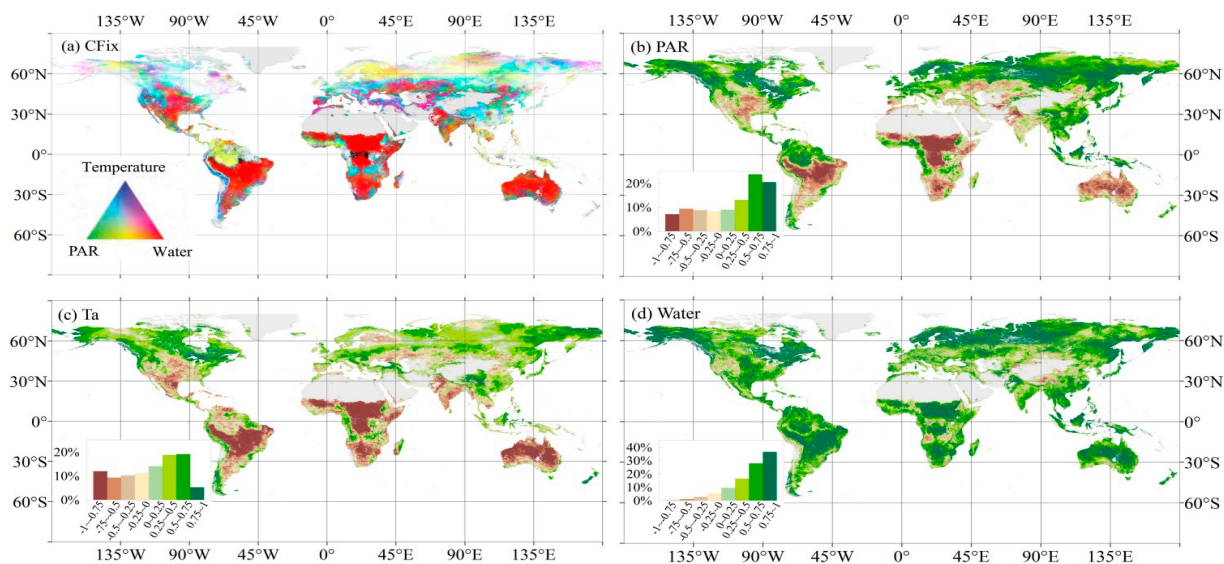
Figure S3. Distribution of climatic constraints to GPP estimated by CFlux model (**a**). Spatial patterns of correlation of annual PAR (**b**); annual mean temperature (**c**); and annual ET (**d**) with annual GPP. (a) is transformed from (b) to (d). The later three data are linearly stretched between 0 and 255, and assigned to Green (radiation (b)), Blue (temperature (c)) and Red (water (d)) for RGB display in (a). The interactions of the three primary color produce: Cyan (temperature and radiation), Magenta (water and temperature) and Yellow (water and radiation).
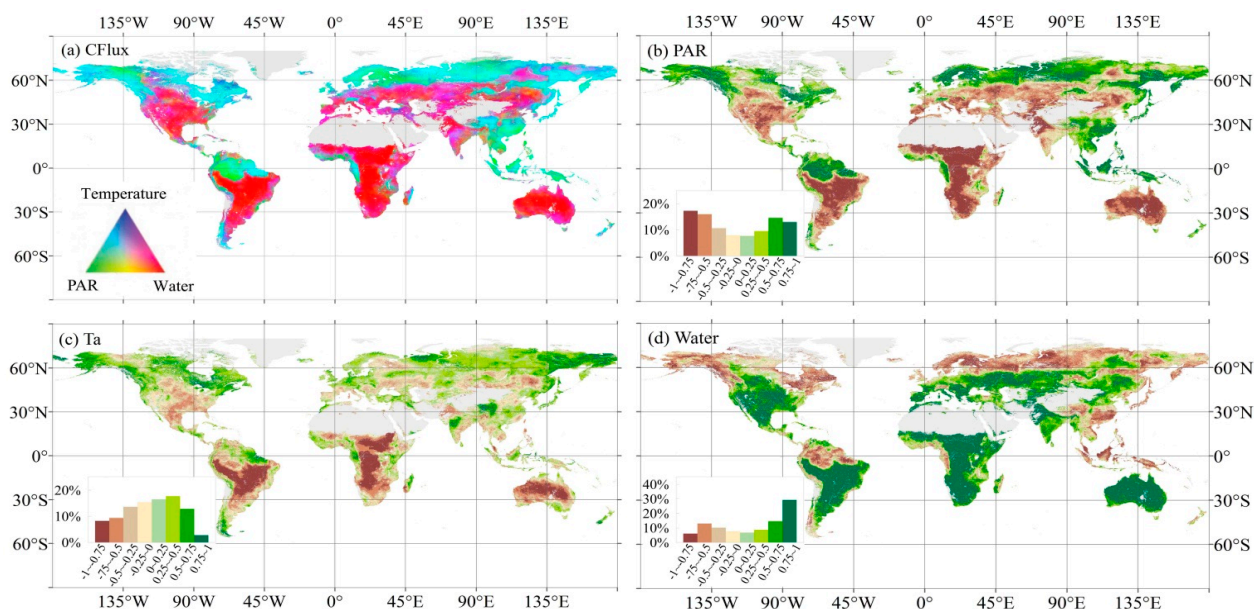
Figure S4. Distribution of climatic constraints to GPP estimated by EC-LUE model (**a**). Spatial patterns of correlation of annual PAR (**b**); annual mean temperature (**c**); and annual ET (**d**) with annual GPP. (a) is transformed from (b) to (d). The later three data are linearly stretched between 0 and 255, and assigned to Green (radiation (b)), Blue (temperature (c)) and Red (water (d)) for RGB display in (a). The interactions of the three primary color produce: Cyan (temperature and radiation), Magenta (water and temperature) and Yellow (water and radiation).
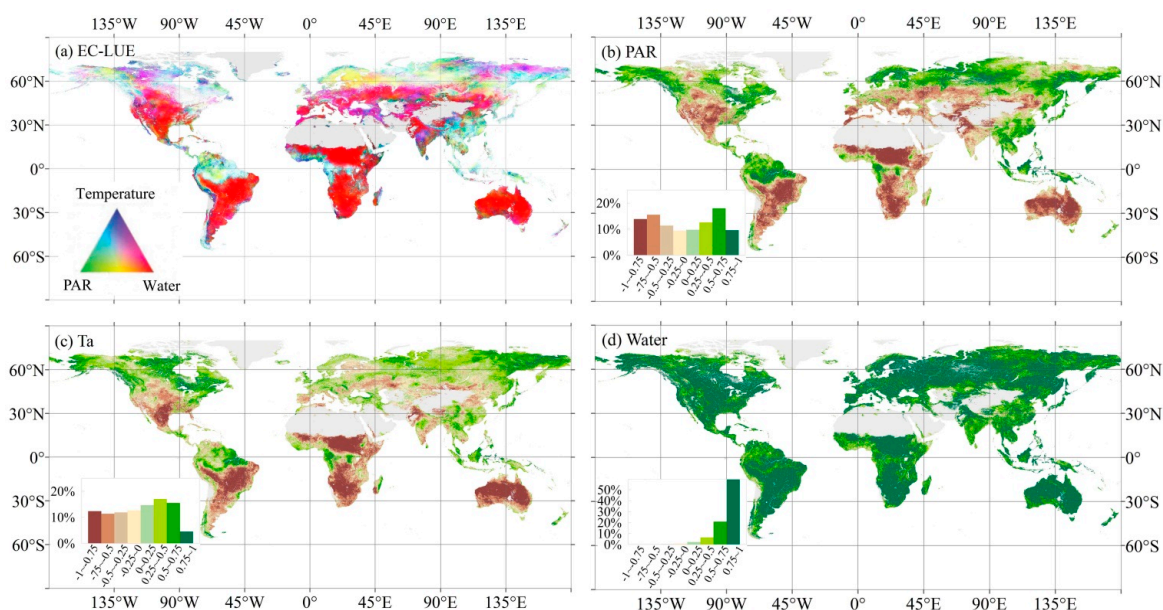
Figure S5. Distribution of climatic constraints to GPP estimated by MODIS model (**a**). Spatial patterns of correlation of annual PAR (**b**), annual mean temperature (**c**); and annual ET (**d**) with annual GPP. (a) is transformed from (b) to (d). The later three data are linearly stretched between 0 and 255, and assigned to Green (radiation (b)), Blue (temperature (c)) and Red (water (d)) for RGB display in (a). The interactions of the three primary color produce: Cyan (temperature and radiation), Magenta (water and temperature) and Yellow (water and radiation).
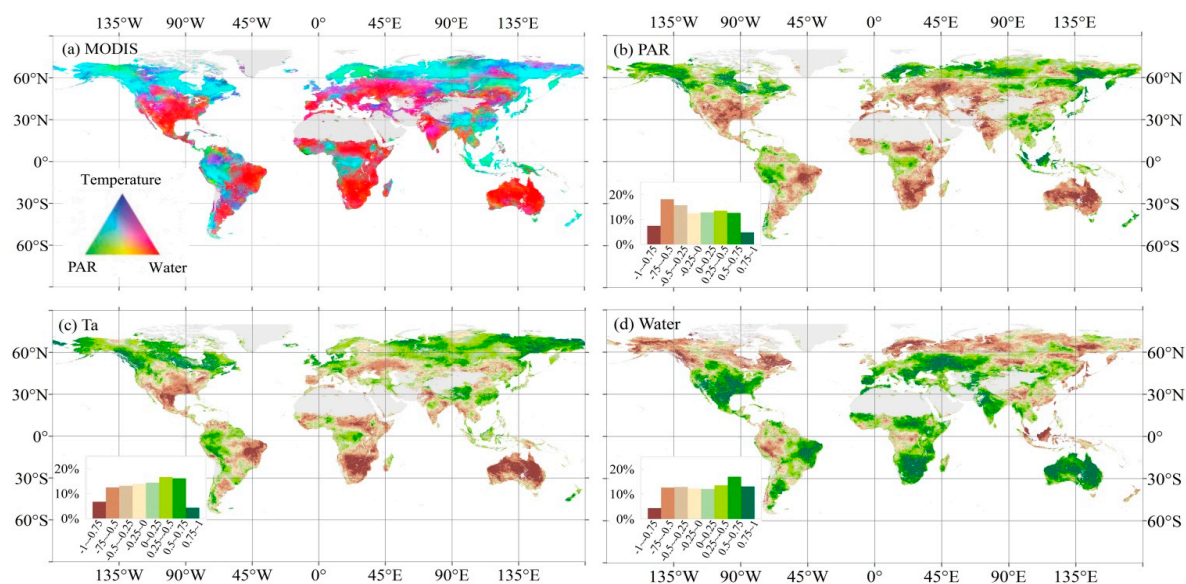
Figure S6. Distribution of climatic constraints to GPP estimated by VPM model (**a**). Spatial patterns of correlation of annual PAR (**b**), annual mean temperature (**c**), and annual ET (**d**) with annual GPP. (a) is transformed from (b) to (d). The later three data are linearly stretched between 0 and 255, and assigned to Green (radiation (b)), Blue (temperature (c)) and Red (water (d)) for RGB display in (a). The interactions of the three primary color produce: Cyan (temperature and radiation), Magenta (water and temperature) and Yellow (water and radiation).
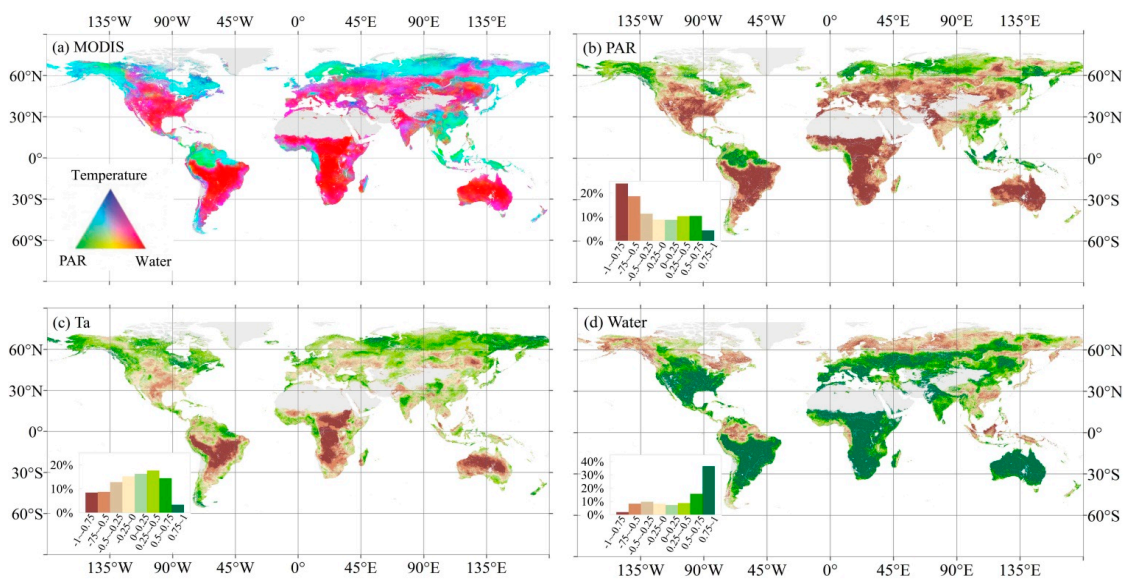
Figure S7. Distribution of climatic constraints to GPP estimated by VPRM model (**a**). Spatial patterns of correlation of annual PAR (**b**), annual mean temperature (**c**), and annual ET (**d**) with annual GPP. (a) is transformed from (b) to (d). The later three data are linearly stretched between 0 and 255, and assigned to Green (radiation (b)), Blue (temperature (c)) and Red (water (d)) for RGB display in (a). The interactions of the three primary color produce: Cyan (temperature and radiation), Magenta (water and temperature) and Yellow (water and radiation).
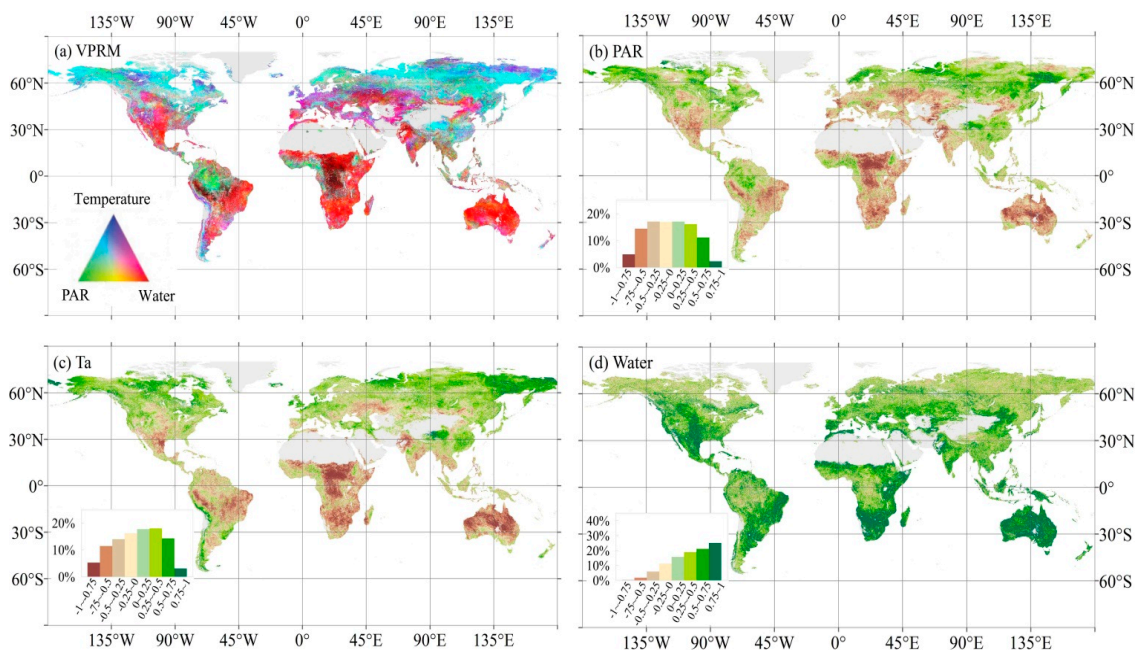
Figure S8. Biomes distribution derived from MODIS land cover product (MCD12Q1). ENF: evergreen needleleaf forest, EBF: evergreen broadleaf forest, DNF: deciduous needleleaf forest, DBF: deciduous broadleaf forest, MIF: mixed forest, SHR: shrubland, SAV: savanna, GRA: grassland, CRO: cropland, DES is no vegetation area.
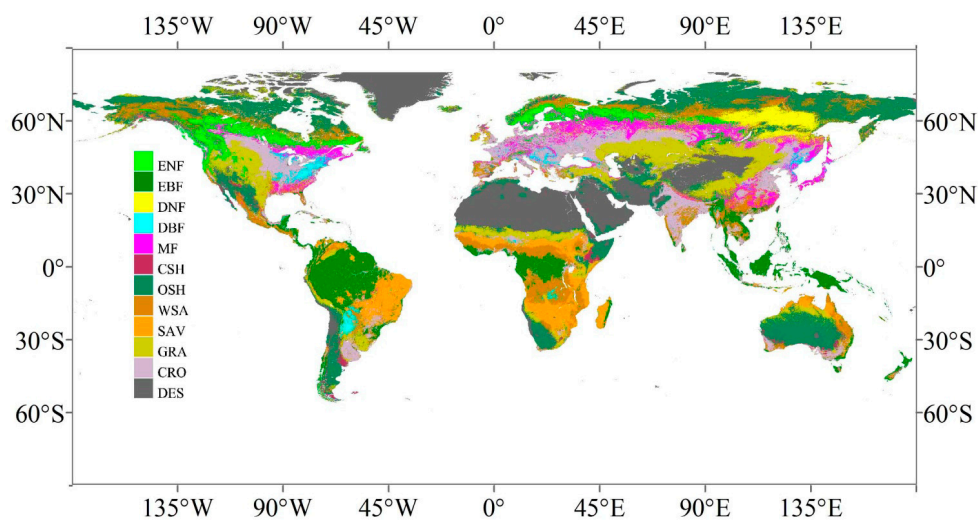
References

S1. Potter, C.S.; Randerson, J.T.; Field, C.B.; Matson, P.A.; Vitousek, P.M.; Mooney, H.A.; Klooster, S.A. Terrestrial ecosystem production: A process model based on global satellite and surface data. *Glob. Biogeochem. Cycles* **1993**, *7*, 811–841.

S2. Veroustraete, F.; Sabbe, H.; Eerens, H. Estimation of carbon mass fluxes over Europe using the C-Fix model and Euroflux data. *Remote Sens. Environ.* **2002**, *83*, 376–399.

S3. Turner, D.P.; Ritts, W.D.; Styles, J.M.; Yang, Z.; Cohen, W.B.; Law, B.E.; Thornton, P.E. A diagnostic carbon flux model to monitor the effects of disturbance and interannual variation in climate on regional NEP. *Tellus* **2006**, *58B*, 476–490.

S4. King, D.A.; Turner, D.P.; Ritts, W.D. Parameterization of a diagnostic carbon cycle model for continental scale application. *Remote Sens. Environ.* **2011**, *115*, 1653–1664.

S5. Yuan, W.; Liu, S.; Zhou, G.; Zhou, G.Y.; Tieszen, L.L.; Baldocchi, D.; Bernhofer, C.; Gholz, H.; Goldstein, A.H.; Goulden, M.L.; *et al*. Deriving a light use efficiency model from eddy covariance flux data for predicting daily gross primary production across biomes. *Agric. For. Meteorol.* **2007**, *143*, 198–207.

S6. Yuan, W.; Liu, S.; Yu, G.; Bonnefond, J.-M.; Chen, J.; Davis, K.; Desai, A.R.; Goldstein, A.H.; Gianelle, D.; Rossi, F.; *et al*. Global estimates of evapotranspiration and gross primary production based on MODIS and global meteorology data. *Remote Sens. Environ.* **2010**, *114*, 1416–1431.

S7. Running, S.W; Neman, R.R.; Heinsch, F.A.; Zhao, M.; Reeves, M.; Hashimoto, H. A continuous satellite-derived measure of global terrestrial primary production. *BioScience* **2004**, *54*, 547–560.

S8. Xiao, X.; Hollinger, D.; Aber, J.; Goltz, M.; Davidson, E.A.; Zhang, Q.; Moore, B., III. Satellite-based modeling of gross primary production in an evergreen needleleaf forest. *Remote Sens. Environ.* **2004**, *89*, 519–534.

S9. Mahadevan, P.; Wofsy, S.C.; Matross, D.M.; Xiao, X.; Dunn, A.L.; Lin, J.C.; Gerbig, C.; Munger, J.W.; Chow, V.Y.; Gottlieb, E.W. A satellite-based biosphere parameterization for net ecosystem CO_2 exchange: Vegetation photosynthesis and respiration model (VPRM). *Glob. Biogeochem. Cycles* **2008**, *22*, GB2005.

S10. Zhang, Y.; Xu, M.; Chen, H.; Adams, J. Global pattern of NPP to GPP ratio derived from MODIS data: Effects of ecosystem type, geographical location and climate. *Glob. Ecol. Biogeogr.* **2009**, *18*, 280–290.

S11. Myneni, R.B.; Williams, D.L. On the relationship between FAPAR and NDVI. *Remote Sens. Environ.* **1994**, *49*, 200–211.

S12. Wang, K.Y. Canopy CO_2 exchange of scots pine and its seasonal variation after four-year exposure to elevated CO_2 and temperature. *Agric. For. Meteorol.* **1996**, *82*, 1–27.

S13. Verstraeten, W.W.; Veroustraete, F.; Feyen, J. On temperature and water limitation of net ecosystem productivity: Implementation in the C-Fix model. *Ecol. Model.* **2006**, *199*, 4–22.

S14. Raich, J.W.; Rastetter, E.B.; Melillo, J.M.; Kicklighter, D.W.; Steudler, P.A.; Peterson, B.J.; Grace, A.L.; Moore, B., III; Vorosmarty, C.J. Potential net primary productivity in South America: Application of a global model. *Ecol. Appl.* **1991**, *1*, 399–429.

S15. Zhang, X.; Friedl, M.A.; Schaaf, C.B.; Strahler, A.H.; Hodges, J.C.F.; Gao, F.; Reed, B.C.; Huete, A. Monitoring vegetation phenology using MODIS. *Remote Sens. Environ.* **2003**, *84*, 471–475.

S16. Yuan, W.; Cai, W.; Xia, J.; Chen, J.; Liu, S.; Dong, W.; Merbold, L.; Law, B.; Arain, A.; Beringer, J.; *et al*. Global comparison of light use efficiency models for simulating terrestrial vegetation gross primary production based on the LaThuile database. *Agric. For.Meteorol.* **2014**, *192–193*, 108–120.